Phonon probe of local strains in SnS_xSe_{2-x} mixed crystals

V. G. Hadjiev,[1] D. De,[2] H. B. Peng,[2] J. Manongdo,[3,4] and A. M. Guloy[3]

[1]*Texas Center for Superconductivity and Department of Mechanical Engineering, University of Houston, Texas 77204-5002, USA*

[2]*Department of Physics and Texas Center for Superconductivity, University of Houston, Texas 77204-5005, USA*

[3]*Department of Chemistry and Texas Center for Superconductivity, University of Houston, Texas 77204-5003, USA*

[4]*Institute of Chemistry, University of the Philippines, Diliman, Quezon City 1101, Philippines*

(Received 4 February 2013; published 15 March 2013)

We present a combined Raman spectroscopy and density functional perturbation theory (DFPT) study of phonon variation with composition x in the mixed crystals SnS_xSe_{2-x}. The experimentally observed two-mode behavior of the A_{1g} and E_g vibrations involving Se(S) atoms is shown to arise from the lack of overlapping of the corresponding phonon dispersion bands in SnS_2 and $SnSe_2$. This offers a unique opportunity to assess local distortions of the trigonal Sn_3Se pyramids in SnS_xSe_{2-x} as no Se and S mode mixing is involved. The dependence of local height and base length of Sn_3Se pyramids with x is derived by a procedure that uses the measured A_{1g} (Se) and E_g (Se) phonons in SnS_xSe_{2-x}, those calculated by DFPT for $SnSe_2$ at different hydrostatic pressure, DFPT phonon dispersion, and the contribution from mass-disorder induced phonon self-energy.

DOI: 10.1103/PhysRevB.87.104302 PACS number(s): 78.30.−j, 71.15.Mb, 63.20.D−

I. INTRODUCTION

The success in both basic research[1,2] and nanoelectronic applications[3] of graphene, a single layer material originally produced as a peel-off of graphite, has triggered a quest for other layered compounds that could be exfoliated down to a single layer. Metal dichalcogenides with the notable representative MoS_2 are among the prospective candidates that can exist as stable single- or few-layer two-dimensional (2D) structures. Molybdenum disulfide reveals much desired three-dimensional (3D) to 2D transition effects as it goes from an indirect 1.3 eV band gap in bulk (multilayered) materials to direct 1.8 eV band gap in a single layer (1L-MoS_2).[4,5] Recently, another member of the metal dichalcogenide family, tin disulfide (SnS_2), has been exfoliated to a few layer crystalline nanomembrane and successfully implemented as a field effect transistor (FET) that is operational at room temperature with a high on/off ratio exceeding 2×10^6 and carrier mobility ~ 1 cm^2 V^{-1} s^{-1}.[6] This achievement has motivated us to revamp the study of SnS_xSe_{2-x} ($0 \leqslant x \leqslant 2$) mixed crystals known to exhibit a linear dependence of the energy band gap with composition x,[7,8] and a variation of carrier density $10^{13} < n(x) < 10^{17}$ and mobility $1 < \mu(x) < 30$ cm^2 V^{-1} s^{-1}.[6,9]

The metal dichalcogenides SnX_2 (X = S, Se) can be grown in various polytype structures.[10] The simplest possible polytype, 2H-SnX_2, crystalizes in a lattice that belongs to the space group $P\bar{3}m1$-D^3_{3d} (No. 164). The hexagonal unit cell (D_{3d}) of 2H-SnX_2 contains one formula unit with two X atoms in-cell and Sn atoms at each of the eight corners of the cell. A fragment of the unit cell confined to a single layer in 2H-SnX_2 (X = S, Se) is shown in the left inset of Fig. 1. Each X atom is covalently bonded to three nearest-neighboring Sn atoms, thus forming a trigonal pyramid Sn_3X. The interaction between the SnX_2 layers in bulk material is weak, perhaps best described by van der Waals force. Alternatively, each Sn atom is octahedrally coordinated to six chalcogen atoms. Since all SnS_xSe_{2-x} ($0 \leqslant x \leqslant 2$) crystals were of 2H polytype we omit 2H specification before composition description throughout the text.

In this paper we present a Raman study of SnS_xSe_{2-x} ($0 \leqslant x \leqslant 2$) mixed crystals complemented by density functional perturbation theory (DFPT) phonon calculations. The local distortions of Sn_3Se trigonal pyramids in SnS_xSe_{2-x} are derived using a procedure that involves the measured Raman active modes in SnS_xSe_{2-x}, DFPT calculated phonon density of states of SnS_2 and $SnSe_2$, and hydrostatic pressure dependence of A_{1g} and E_g modes in $SnSe_2$. The mass-disorder phonon self-energy is also taken into account.

II. MATERIAL PREPARATION, CHARACTERIZATION, AND RAMAN EXPERIMENT

Few to a hundred micron sized SnS_xSe_{2-x} single crystals were grown in quartz ampules by reacting stoichiometric mixture of the pure elements via chemical vapor transport (CVT), using iodine as the transport agent as described in Refs. 6 and 11. Each loaded ampule was evacuated, sealed under vacuum ($<1 \times 10^{-4}$ Pa), and heated in a two-zone furnace with the reactants placed at the hot end of the furnace T_h, thus enabling the composition mixture to be transported and grown in the cooler end of the furnace T_c. The vapor transport reactions were kept active in the furnace for 12 h and then air-cooled by shutting off the furnace. The temperature settings for growing crystals of each of the SnS_xSe_{2-x} compositions as well as the corresponding lattice parameters measured with a x-ray diffractometer (PANalytical XPert PRO MRD, Cu-$K\alpha$ radiation) are given in Table I. The a and c lattice constants in Table I deviate by less than 0.5% from those reported in an earlier experimental study of structural and vibrational properties of SnS_xSe_{2-x}.[12]

The Raman scattering spectra of platelike SnS_xSe_{2-x} single crystals were measured under an optical microscope (objective ×50 magnification) attached to a Horiba JY T64000 triple spectrometer. All spectra are recorded in backscattering configuration with the 514.5 nm laser excitation and incident and scattered light propagating along the c axis of the crystals.

TABLE I. Hot (T_h) and cool (T_c) end furnace temperatures for growing SnS_xSe_{2-x} crystals, the corresponding lattice parameters of the hexagonal $P\bar{3}m1$ structure (unit cell angles: $\alpha = \beta = 90^\circ$, $\gamma = 120^\circ$), and measured A_{1g} and E_g phonon frequencies.

Parameters	$x = 0.0$	$x = 0.4$	$x = 0.8$	$x = 1.2$	$x = 1.6$	$x = 2.0$
T_h, °C	550	580	605	635	662	690
T_c, °C	510	535	565	590	618	645
a, Å	3.815(1)	3.783(1)	3.7415(6)	3.7060(7)	3.6802(7)	3.6513(7)
c, Å	6.144(2)	6.117(1)	6.076(2)	6.021(2)	5.971(2)	5.902(1)
A_{1g}(Se), cm^{-1}	185.9	189.9	200.0	205.1	206.5	
E_g(Se), cm^{-1}	118.9	123.1	130.8	139.4	149.5	
A_{1g}(S), cm^{-1}			298.3	304.4	309.6	313.9
E_g(S), cm^{-1}			178.3	189.0	191.0	205.4

III. EXPERIMENTAL RESULTS

Figure 1 shows the unpolarized Raman spectra of SnS_xSe_{2-x} for all six available compositions. Each unpolarized spectrum is an average of two spectra taken from the same spot, one measured with parallel incident and scattered light polarizations and the other in crossed polarizations. The frequency of Raman lines and relative intensities are in good agreement with those reported in literature.[9,12–14]

The three-atom unit cell of SnX_2 (X = S, Se) gives rise to nine vibrational modes. Sn and S(Se) atoms occupy $1a$ and $2d$ Wyckoff positions in the $P\bar{3}m1$ crystal structure, respectively. Group theoretical symmetry analysis[15] yields the irreducible representations of the Γ-point phonon modes: $\Gamma = A_{1g} + 2A_{2u} + E_g + 2E_u$. The acoustic modes are $A_{2u} + E_u$ and of the four optical modes two, $A_{2u} + E_u$, are infrared active and the other two, $A_{1g} + E_g$, Raman active modes. Since only $2d$ cite symmetry, occupied by chalcogen atoms in the cell, contributes to the Raman modes, A_{1g} and E_g species involve exclusively S(Se) vibrations. The A_{1g} and E_g symmetries are easily distinguished experimentally. The A_{1g} mode intensity diminishes in crossed incident and scattered light polarizations for backscattering along the c axis of the crystals because in its Raman tensor only the diagonal elements are nonzero.

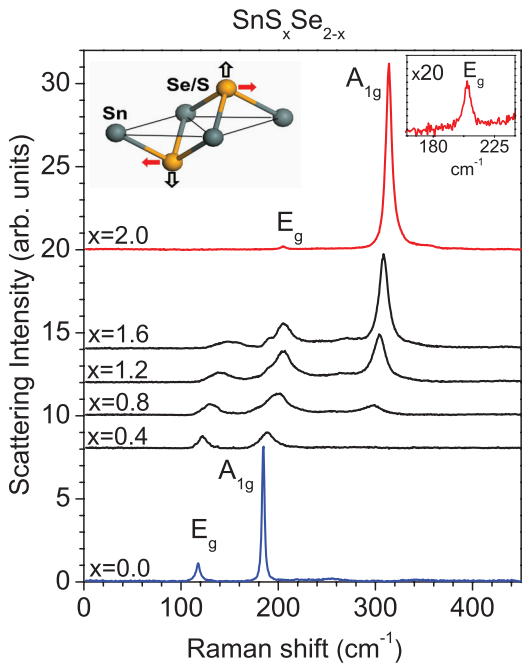

FIG. 1. (Color online) Raman spectra of SnS_xSe_{2-x} excited with 514.5 nm laser line. The left inset shows the eigenvector of the A_{1g} (black contour arrow) mode and one of the two eigenvectors belonging to the E_g (red solid arrow) mode. The other E_g eigenvector is orthogonal, out-of-plane, to that in the picture. The right inset shows a magnified portion of $x = 2.0$ (SnS_2) spectrum around the E_g mode.

The large separation between experimental Raman mode frequencies in SnS_2 and $SnSe_2$ seen in Table I comes mostly from the big difference between S and Se atomic masses, $(m_{Se}/m_S)^{1/2} \approx 1.57$, through the mass dependence $\omega_S \sim (m_{Se}/m_S)^{1/2}\omega_{Se}$. A brief comparison of experimental frequencies in Table I, however, shows that the mass dependence alone cannot describe the Raman frequency change in going from SnS_2 to $SnSe_2$.

The most important piece of information that Fig. 1 conveys is the two-mode behavior of A_{1g} and E_g phonons in the mixed crystals. Note that the relative intensity of the E_g mode in SnS_2 is very weak as shown in the right inset in Fig. 1 and the trace of this mode vanishes in the Raman spectrum for $x = 0.4$. On the other hand, the frequencies of S and Se Raman modes shift with composition in a direction that could be compatible with one-mode behavior $\omega_{Se}(2 - x) \sim (m_{Se}/\bar{m}_{Se_{2-x}})^{1/2}\omega_{Se}$, where $\bar{m}_{Se_{2-x}} = \{[(1 - 0.5x) \cdot m_{Se} + 0.5x \cdot m_S]\}^{1/2}$. Therefore, the evolution of Raman modes with composition x in SnS_xSe_{2-x} can be explained either as a result of mixed-mode (combined one- and two-mode) behavior or the mixed crystal system exhibits two-mode behavior but the frequency change with x is due to the local strain of Sn_3Se and Sn_3S pyramids.

The strain-induced shift of Raman frequencies in the two-mode behavior $GaAs_{0.77}P_{0.23}$ and $GaAs_{0.9}P_{0.1}$ thin films was studied in Ref. 16. The different level of residual strain in these films was created by growing layers of fixed composition and different thickness. Based on their Raman spectroscopy with x-ray diffraction results, the authors of Ref. 16 obtained a phenomenological coefficient of proportionality between the fractional Raman frequency change and in-plane film strain. This approach, however, has limited applicability to the SnS_xSe_{2-x} system in which the strains of Sn_3Se and Sn_3S components vary with composition.

One approach for predicting the behavior (one, two, or mixed mode) of a phonon with given symmetry and eigenvector in mixed crystals is to compare the phonon dispersion in

the end compositions. A clean two-phonon behavior is realized when no overlapping of the corresponding dispersions occurs for all phonon wave vectors. To investigate whether the lattice dynamics calculations supported the two-mode behavior of the Raman phonons in SnS_xSe_{2-x}, we calculated the phonon dispersion in SnS_2 and $SnSe_2$ using a density functional perturbation theory (DFPT) code.[17]

IV. DFPT CALCULATION DETAILS

The calculations were performed within the generalized-gradient approximation (GGA) with Revised-Perdew-Burke-Ernzerhof (RPBE) exchange-correlation functional[18] using the norm-conserved pseudopotential plane-wave method.[17] The electronic band structure, related properties, and geometry optimization of the structures were calculated self-consistently (SCF) with 720 eV kinetic energy cutoff for the plane waves and SFC tolerance better than 5×10^{-7} eV/atom over $5 \times 5 \times 2$ Monkhorst-Pack grid in the k space. The geometry optimization of the unit cell was done within the BFGS[19] energy minimization scheme with fully relaxed structure and varied number of plane waves to maintain fixed energy cutoff. During minimization the maximum deviation from crystal symmetry was constrained to 1×10^{-8} Å until completed with convergence parameters better than 2×10^{-6} eV per atom for energy, 8×10^{-3} eVÅ^{-1} for forces, 0.02 GPa for stresses, and 5×10^{-4} Å for displacements. The calculated a lattice constant deviates from the experiential one by -0.8% and -0.25% for SnS_2 and $SnSe_2$ structures, respectively.

The band structure calculations of SnS_2 and $SnSe_2$ reveal nonmetallic systems with indirect band gaps 2.1 and 1.1 eV, respectively, in good agreement with the experiment.[9] This allowed us to use the linear response DFTP code[20,21] in the phonon calculations. The phonon dispersion was calculated within an interpolation scheme over $32 \times 32 \times 16$ Monkhorst-Pack mesh with q-vector separation 0.01 Å^{-1} and convergence tolerance 1×10^{-5} eV Å^{-2} for the electronic eigenvalues during the phonon calculations. The response of the SnS_2 and $SnSe_2$ structures to electric field was also calculated in order to make a nonanalytical correction to the dynamic matrix elements and thus to calculate the LO/TO (longitudinal to transversal) phonon splitting of infrared (IR) modes. It is important to note that the calculated phonon frequencies for 2H-polytype of SnS_2 and $SnSe_2$ differ less than 0.5% from the corresponding ones of single layered (1L) structures, i.e., interlayer interactions are very weak.

Figure 2 shows the phonon dispersion in SnS_2 (blue solid line) and $SnSe_2$ (red solid circles) including the LO/TO splitting of the E_u modes along the high symmetry directions in the Brillouin zone. The double degenerate E_u mode has two orthogonal eigenvectors, which results in LO/TO splitting when the phonon propagates in the ab plane. The calculated LO/TO splitting of the E_u modes at Γ point as well as A_u(LO) and A_u(TO) frequency difference for SnS_2 and $SnSe_2$ are in remarkable agreement with the experiment.[9,13] The calculated A_{1g} and E_g phonon eigenvectors are displayed in the left inset of Fig. 1. As expected, the eigenvectors are simple and involve only the chalcogen vibrations. The A_{1g} and E_g dispersion bands in SnS_2 and $SnSe_2$ are well separated from each other,

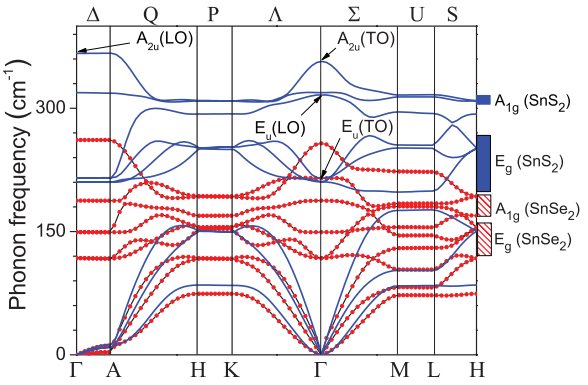

FIG. 2. (Color online) DFPT-calculated phonon dispersion in SnS_2 (blue solid line) and $SnSe_2$ (red solid circle). Note the lack of overlapping of corresponding A_{1g} and E_g mode dispersion in both compounds. The LO/TO splitting of E_u modes closely reproduces the experimentally measured one in Refs. 9 and 13.

which is indicative of two-mode behavior of the Raman active phonons.

V. DISCUSSION

We explore the change of Raman phonon frequencies with x in SnS_xSe_{2-x}. The $Sn_3S(Se)$ pyramid shown in Fig. 1 is the smallest unit taking part in the A_{1g} and E_g modes of S(Se) vibrations. A comparison of SnS_xSe_{2-x} lattice constants in Table I gives a gradual decrease of both a and c lattice constants in going from $SnSe_2$ ($x = 0$) to SnS_2 ($x = 2.0$). Therefore in the mixed crystals the Sn_3Se pyramids experience local compressive strain and Sn_3S ones are subjected to tensile strain. Since only Sn_3Se is under compression, one feasible way to assess the local strain is to find out those lattice parameters of $SnSe_2$ under hydrostatic pressure that yield Raman phonon frequencies equal to the experimental ones. At this point we note that to the best of our knowledge there is no reported experimental or theoretical work on the $SnSe_2$ Raman modes dependence with hydrostatic pressure.

For the purpose of understanding pressure dependence, we used DFPT to calculate the Raman mode frequencies of $SnSe_2$ at simulated hydrostatic pressure ranging from 0 to 10 GPa. This type of calculations are usually successful only after a very good optimization of the crystal structure at a given pressure, which we achieve with the above reported calculation accuracy. The advantage of these calculations is that for a given set of Raman data one obtains also a detailed crystal structure information including the base length and height of the Sn_3Se pyramids. Figure 3 compares the fractional A_{1g}(Se) and E_g(Se) frequency variation with the change of the average a lattice constant (x-ray measured) in SnS_xSe_{2-x} (open symbols) and that with calculated at different hydrostatic pressure (closed symbols). The presented data shows that the calculated fractional phonon frequencies under pressure increase with the a strain ($-\Delta a/a_0$) faster than those experimentally obtained for SnS_xSe_{2-x}. This result is intuitively understandable. As sulfur content in the mixed crystal increases, the average a lattice constant decreases but local Sn_3Se pyramid base length shortening is lagging. As a result we find that each experimental Raman frequency corresponds to a lower strained

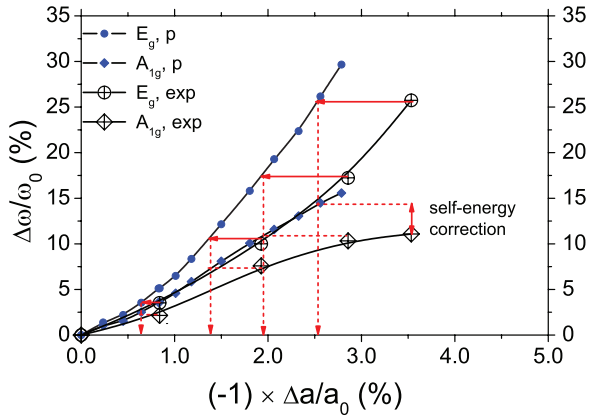

FIG. 3. (Color online) Experimental and calculated fractional phonon frequency ($\Delta\omega/\omega_0$) dependence of Se modes as a function of fractional change of the a lattice constant driven by chemical pressure (large open circles and rhombi) or hydrostatic pressure in DFPT simulation (small solid blue circles and rhombi). The red arrows guide the procedure of finding local $\Delta a/a_0$ for the Sn_3Se pyramids in SnS_xSe_{2-x}.

$SnSe_2$ structure under hydrostatic pressure. The horizontal solid arrows in Fig. 3 relate the experimental E_g frequency data to the hydrostatic one. Remarkably, the vertical dashed arrows cross the hydrostatic A_{1g} data at phonon frequencies very close to the corresponding experiential values. The significance of these results is that based on achieved consistency of the experimental and computed data we can derive the local strain of the Sn_3Se pyramid base at the points the dash arrows cross the $-\Delta a/a_0$. Once we find the hydrostatically compressed $SnSe_2$ crystal structure producing the experimental Raman mode frequencies we can obtain also the corresponding change of the Sn_3Se pyramid.

Now we discuss the apparent deviation of the experimental fractional A_{1g} frequency $\Delta\omega/\omega_0 \sim 11.1\%$ from the calculated 14.5% at $-\Delta a/a_0 \sim 2.5\%$ as seen in Fig. 3. The deviation can be related to the well known disorder-induced phonon self-energy effects.[22–24] The atomic disorder can be described by a disorder Hamiltonian that renormalizes the harmonic excitation (phonon). Treating the disorder by perturbation theory and under assumption that its contribution adds linearly to to the harmonic one and thus can be calculated separately, one can write the additional phonon self-energy $\Sigma(\omega)$ as

$$\Sigma_{\rm dis}(\omega) = \Delta_{\rm dis}(\omega) - \mathbf{i}\Gamma_{\rm dis}(\omega), \tag{1}$$

where $\Delta_{\rm dis}(\omega_p)$ is the self-energy addition to the bare phonon frequency ω_p (without disorder) in our case the one calculated at a given hydrostatic pressure, i.e., $\omega_{\rm exp} = \omega_p + \Delta_{\rm dis}(\omega_p)$. The imaginary part of Eq. (1) gives the corresponding contribution to the phonon linewidth $\Gamma_{\rm exp} = \Gamma_{SnSe_2} + \Gamma_{\rm dis}(\omega_p)$. Most of the existing models treat only the isotope mass disorder in mixed crystals.[22–24] We apply here such an approach merely to estimate the contribution from the mass disorder introduced by chalcogen substitution in SnS_xSe_{2-x}, noting the limitations imposed by neglecting the changes of force constants.

In second-order perturbation theory,[22–24] the expression for mass disorder-induced frequency shift and line broadening (FWHM) of the A_{1g} and E_g Raman lines of Se in a predominant SnS_2 lattice read

$$\Delta_{\rm dis}(\omega) = \frac{1}{12} g_2 \omega^2 P \int_0^\infty \frac{\omega' \rho_1(\omega')}{\omega^2 - \omega'^2} d\omega', \tag{2}$$

$$\Gamma_{\rm dis} = \frac{\pi}{24} g_2 \omega^2 \rho_1(\omega), \tag{3}$$

and

$$g_2 = \left(1 - \frac{x}{2}\right)\left(\frac{m_{\rm Se} - \bar{m}}{\bar{m}}\right)^2, \tag{4}$$

where $\rho_1(\omega)$ is the one-phonon density of states of SnS_2 normalized to the number of all modes, $3N_{\rm cell} = 9$, P is the principle part of the Cauchy integral, g_2 is the second moment of the mass fluctuations, and $\bar{m}$ the average mass for composition x, $\bar{m} = (x/2)m_{\rm S} + (1 - x/2)m_{\rm Se}$. The square of the eigenvector of A_{1g} and E_g modes, $|\mathbf{e}_{A_{1g},E_g}|^2 = 1/2$, is also accounted for in Eqs. (2) and (3).

The frequency dependence of mass-disorder induced self-energy of Se modes in $SnS_{1.6}Se_{0.4}$ is shown in Fig. 4. The corresponding curves were calculated using Eqs. (2)–(4) and DFPT calculated one-phonon density of states of SnS_2. The experimental Raman frequencies and linewidths $\omega_{\rm exp}/\Gamma_{\rm exp}$ in $SnS_{1.6}Se_{0.4}$ are 149.5/29 and 206.5/21 cm^{-1} (see Table I and Fig. 1) for the E_g and A_{1g} modes, respectively. The corresponding calculated at hydrostatic pressure frequency ω_p of the A_{1g} bare phonon is 213 cm^{-1}, whereas that of E_g is 148 cm^{-1}, i.e., close to the experimental one. In Fig. 4 one finds that $\Delta_{\rm dis}(A_{1g}) = -5$ cm^{-1}, which fulfils well the equity $\omega_{\rm exp} = \omega_p + \Delta_{\rm dis}(\omega_p)$. Given the very narrow lines of Se vibrations in $SnSe_2$, $\Gamma_{\rm exp}(E_g) = 6\,cm^{-1}$ and $\Gamma_{\rm exp}(A_{1g}) = 3\,cm^{-1}$, the calculated $\Gamma_{\rm dis}(A_{1g}) = 7\,cm^{-1}$ is not sufficient to explain the experimental broadening of 18 cm^{-1}. The same conclusion is valid also for $\Gamma_{\rm dis}(E_g) = 1$ cm^{-1} versus the experimental broadening of 23 cm^{-1}. The E_g phonon exhibits negligible phonon self-energy effects.

These results indicate that additional disorder effects may take place as well. For instance, the calculated $\Gamma_{\rm dis}$ represents a homogeneous Raman line broadening due to a decrease of

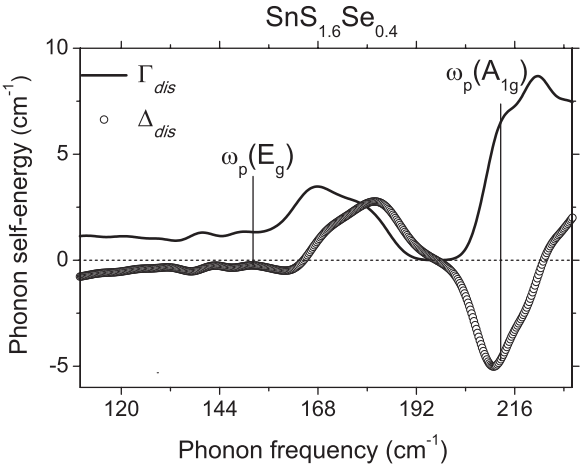

FIG. 4. Real ($\Delta_{\rm dis}$, frequency shift) and imaginary ($\Gamma_{\rm dis}$, line broadening) parts of disorder-induced phonon self-energy of Se vibrations in $SnS_{1.6}S_{0.4}$ calculated using the one-phonon density of states of SnS_2 and $g_2 = 0.1633$ ($x = 1.6$). The "bare" phonon frequencies $\omega_p(E_g)$ and $\omega_p(A_{1g})$ are those calculated at hydrostatic pressure that results in $-\Delta a/a_0 \sim 2.5\%$.

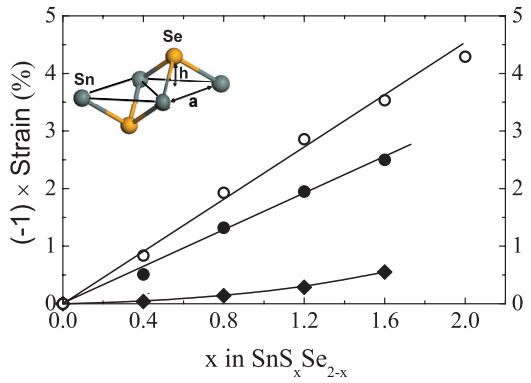

FIG. 5. (Color online) Distortion of $SnSe_3$ pyramids with x in SnS_xSe_{2-x}. The solid circles and rhombi denote the fractional change of the base length a $(-\Delta a/a_0)$ and height h $(-\Delta h/h_0)$, respectively, of Sn_3Se pyramids with x. Open circles traces the fractional change of average, x-ray measured, a lattice constant with x.

phonon lifetime caused by elastic phonon scattering. On the other hand, different size Sn_3Se clusters in SnS_xSe_{2-x} experience different strain and their phonon frequencies vary. This effect causes an inhomogeneous broadening and the phonon line shape is an envelope of the frequency distribution. We relate the additional broadening to inhomogeneous broadening due to differently strained Sn_3Se structures in SnS_xSe_{2-x}. A more detailed treatment should involve fitting of the E_g Raman line by a Voigt profile function[25] representing a convolution of Gaussian frequency distribution of Lorentzians with linewidths equal to that in $SnSe_2$. In reality, however, the E_g line shape in SnS_xSe_{2-x} may have a more complex form due to specific distribution of S and Se in the measured crystal, and this part of the analysis should be done on a case-by-case basis.

Finally, based on (i) the findings in Fig. 3 that the experimental A_{1g} and E_g frequencies for a given $x = 0.4$ to $x = 1.2$ correspond to a close frequency pair of modes calculated at the same hydrostatic pressure, and (ii) the disorder-induced phonon-self energy of the E_g mode in SnS_xSe_{2-x} is negligibly small (Fig. 4), we relate the experimental E_g frequencies to calculated under simulated hydrostatic pressure structures using the solid blue circle curve in Fig. 3. Following this procedure we plot in Fig. 5 the dependence of base length (solid circles) and height (solid rhombi) of the Sn_3Se pyramids in SnS_xSe_{2-x}. The open circle data shows the average strain of the a lattice constant in SnS_xSe_{2-x} with respect to the a parameter in $SnSe_2$. Therefore, Fig. 5 can serve as a master curve that could provide an assessment of Sn_3Se pyramid distortions with x in SnS_xSe_{2-x}.

VI. CONCLUSIONS

The variation of Raman phonon frequencies and linewidths with x in SnS_xSe_{2-x} was studied experimentally and by DFPT first-principle calculations. A practical procedure for measuring the strain and strain distribution of Sn_3Se in SnS_xSe_{2-x} is suggested that involves Raman spectroscopy measurements and assessment of the local strain of Sn_3Se pyramids from the master curves plotted in Fig. 5. The strain distribution for a given composition x can be obtained from the E_g(Se) phonon line shape (showing negligible disorder-induced phonon self-energy) after deconvolution with the intrinsic E_g line measured in $SnSe_2$.

ACKNOWLEDGMENTS

This work was supported by the State of Texas through the Texas Center for Superconductivity (TcSUH) at the University of Houston, NSF-ECCS (Award No. ECCS-1247874). J.M. and A.M.G. also acknowledge support from the R. A. Welch Foundation (E-1297).

[1] K. S. Novoselov, A. K. Geim, S. V. Morozov, D. Jiang, M. I. Katsnelson, I. V. Grigorieva, S. V. Dubonos, and A. A. Firsov, Nature (London) **438**, 197 (2005).
[2] Y. Zhang, Y-W. Tan, H. Stormer, and P. Kim, Nature (London) **438**, 201 (2005).
[3] K. S. Novoselov, A. K. Geim, S. V. Morozov, D. Jiang, Y. Zhang, S. Dubonos, I. V. Grigorieva, and A. A. Firsov, Science **306**, 666 (2004).
[4] A. Splendiani, L. Sun, Y. Zhang, T. Li, J. Kim, C.-Y. Chim, G. Galli, and F. Wang, Nano Lett. **10**, 1271 (2010).
[5] K. F. Mak, C. Lee, J. Hone, J. Shan, and T. F. Heinz, Phys. Rev. Lett. **105**, 136805 (2010).
[6] D. De, J. Manongdo, S. See, V. Zhang, A. Guloy, and H. B. Peng, Nanotechnology **24**, 025202 (2013).
[7] P. A. Lee, G. Said, R. Davis, and T. H. Lim, J. Phys. Chem. Solids **30**, 2719 (1969).
[8] F. Aymerich, F. Meloni, and G. Mula, Solid State Commun. **12**, 139 (1973).
[9] C. Julien, M. Eddrief, I. Samaras, and M. Balkanski, Mater. Sci. Eng. B **15**, 70 (1992).
[10] B. Pałosz and E. Salje, J. Appl. Crystallogr. **22**, 622 (1989).
[11] F. Al-Alamy and A. Balchin, J. Cryst. Growth. **38**, 221 (1977).
[12] A. K. Garg, J. Mol. Struct. **247**, 47 (1990).
[13] G. Lucovsky, J. C. Mikkelsen, W. Y. Liang, R. M. White, and R. M. Martin, Phys. Rev. B **4**, 1663 (1976).
[14] A. J. Smith, P. E. Meek, and W. Y. Liang, J. Phys. C **10**, 1321 (1977).
[15] D. L. Rousseau, R. P. Bauman, and S. P. S. Porto, J. Raman Spectrosc. **10**, 253 (1981).
[16] G. Armelles, M. J. Sanjuán, L. González, and Y. González, Appl. Phys. Lett. **68**, 1805 (1996).
[17] S. J. Clark, M. D. Segal, C. J. Packard, P. J. Hasnip, M. I. J. Probert, K. Refson, and M. C. Payne, Z. Kristallogr. **220**, 567 (2005).
[18] B. Hammer, L. B. Hansen, and J. K. Norskov, Phys. Rev. B **59**, 7413 (1999).
[19] B. G. Pfrommer, M. Cote, S. G. Louie, and M. L. Cohen, J. Comput. Phys. **131**, 133 (1997).
[20] K. Refson, P. R. Tulip, and S. J. Clark, Phys. Rev. B **73**, 155114 (2006).
[21] S. Baroni, S. de Gironcoli, A. dal Corso, and P. Giannozzi, Rev. Mod. Phys. **73**, 515 (2001).
[22] S. I. Tamura, Phys. Rev. B **27**, 858 (1983).
[23] M. Cardona and T. Ruf, Solid State Commun. **117**, 201 (2001).
[24] V. G. Plekhanov, Phys. Rep. **410**, 1 (2005).
[25] B. H. Armstrong, J. Quant. Spectrosc. Radiat. Transfer **7**, 61 (1967).